BIOCHEMISTRY
including biophysical chemistry & molecular biology

Article

pubs.acs.org/biochemistry

Light-Induced Subunit Dissociation by a Light−Oxygen−Voltage Domain Photoreceptor from *Rhodobacter sphaeroides*

Karen S. Conrad, Alexandrine M. Bilwes, and Brian R. Crane*

Department of Chemistry and Chemical Biology, Cornell University, Ithaca, New York 14853, United States

Supporting Information

ABSTRACT: Light−oxygen−voltage (LOV) domains bind a flavin chromophore to serve as blue light sensors in a wide range of eukaryotic and prokaryotic proteins. LOV domains are associated with a variable effector domain or a separate protein signaling partner to execute a wide variety of functions that include regulation of kinases, generation of anti-sigma factor antagonists, and regulation of circadian clocks. Here we present the crystal structure, photocycle kinetics, association properties, and spectroscopic features of a full-length LOV domain protein from *Rhodobacter sphaeroides* (RsLOV). RsLOV exhibits N- and C-terminal helical extensions that form an unusual helical bundle at its dimer interface with some resemblance to the helical transducer of sensory rhodopsin II. The blue light-induced conformational changes of RsLOV revealed from a comparison of light- and dark-state crystal structures support a shared signaling mechanism of LOV domain proteins that originates with the light-induced formation of a flavin−cysteinyl photoadduct. Adduct formation disrupts hydrogen bonding in the active site and propagates structural changes through the LOV domain core to the N- and C-terminal extensions. Single-residue variants in the active site and dimer interface of RsLOV alter photoadduct lifetimes and induce structural changes that perturb the oligomeric state. Size exclusion chromatography, multiangle light scattering, small-angle X-ray scattering, and cross-linking studies indicate that RsLOV dimerizes in the dark but, upon light excitation, dissociates into monomers. This light-induced switch in oligomeric state may prove to be useful for engineering molecular associations in controlled cellular settings.

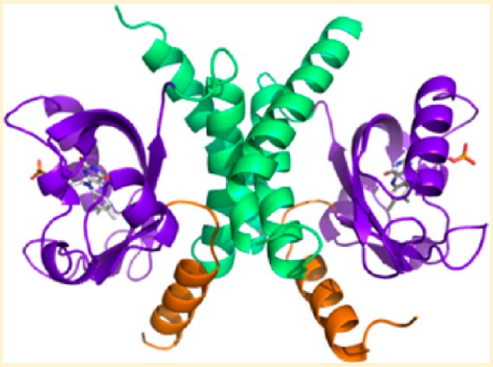

Per-ARNT-Sim (PAS) domains are key components of many photoreceptor proteins and are present in all kingdoms of life.[1] PAS domains often detect signals through a cofactor that undergoes chemical changes in response to environmental stimuli.[2,3] Light−oxygen−voltage (LOV) domains are a subset of the PAS domain superfamily that exhibit a mixed α/β-fold common to PAS domains but are distinguished by binding a flavin cofactor that imparts blue-light (λ = 440−480 nm) sensitivity.[4,5] LOV domains serve as sensory domains that modulate interactions in signal transduction proteins. Upon photoexcitation by blue light, the noncovalently bound flavin cofactor forms a covalent adduct between the flavin C4a atom and the sulfur atom of a conserved cysteine residue in the LOV domain active center (Figure 1).[6]

LOV domain proteins perform many different functional roles that are determined by an associated effector domain or protein partner under control of the LOV light switch. These roles include the regulation of the phototropin serine/threonine kinases (phot1 and phot2) in *Chlamydomonas reinhardtii* (green algae)[7,8] and higher plant life, *Oryza sativa* (rice),[9−11] regulation of histidine kinases in *Caulobacter crescentus* (Gram-negative bacterium),[12,13] regulation of the anti-sigma factor antagonist YtvA in *Bacillus subtilis* (Gram-positive bacterium),[14−17] and regulation of the circadian clock photosensors White collar-1 (WC-1) and Vivid (VVD) in *Neurospora crassa* (filamentous fungi),[18−22] (Figure 1).[23] LOV domain proteins that do not contain an effector domain are so-called "short" LOV domains.[24] Short LOV domain proteins include VVD and the LOV domain protein from *Pseudomonas putida* (PpSB1-LOV)[25] as well as the LOV protein of this work from *Rhodobacter sphaeroides*. VVD has been shown to signal to a protein partner in the White-Collar Complex.[26−28] Thus, LOV domains propagate signals in two distinct ways: by affecting an auxiliary domain within the LOV protein or by interactions with a protein partner.

Outside of the conserved structural core,[29] LOV domains are distinguished by variations of their N- and C-terminal structural extensions (Figure 2). These structural differences result in a variety of molecular mechanisms in light-dependent signaling of LOV proteins. A key attribute of LOV domains is their tendency to dimerize. There are two general association modes of PAS−PAS dimerization. In one mode, the dimer interface is the PAS domain β-scaffold, as seen in hypoxia inducible factor,[30] KinA histidine kinases,[31] and LOV1-type proteins.[32] In the second mode, the N-terminal helices flanking the domain core (Ncap) of each subunit form intermolecular contacts that establish the dimer interface. This mode is exhibited by heme-based oxygen sensor FixL,[33] nitrogen fixation regulatory protein NifL,[34] and heme-regulated phosphodiesterase *Ec*DOS.[35] Interestingly, the LOV domain protein VVD exhibits the

Received: August 2, 2012
Published: December 19, 2012

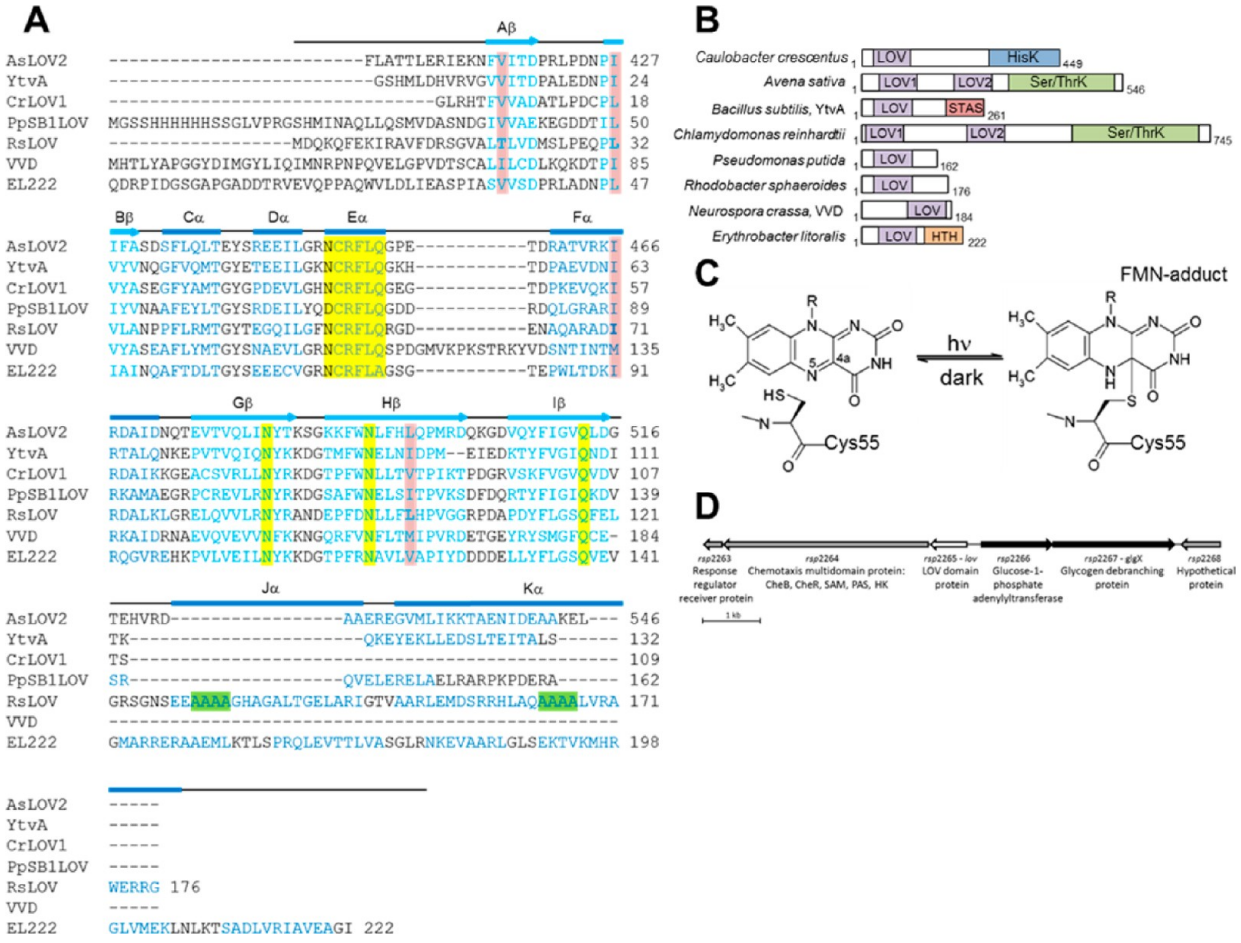

Figure 1. LOV domain homology and chemistry. (A) Structure-based sequence alignment of LOV domains: *Avena sativa* LOV2 (2V1A), *B. subtilis* (2PR5), *C. reinhardtii* (1N9L), *P. putida* (3SW1), *R. sphaeroides* (RsLOV), *N. crassa* Vivid (2PD7), and *Erythrobacter litoralis* (3P7N). Secondary structure elements are noted above (α-helical residues colored blue, β-sheets colored aqua). Residues critical to flavin coordination are highlighted in yellow; sites of RsLOV single-residue variants surrounding the FMN-binding pocket are highlighted in pink, and the four-Ala repeats in helices Jα and Kα are highlighted in green. (B) Domain arrangement of sequence-aligned LOV domain proteins (number of residues specified). Abbreviations: HisK, histidine kinase; Ser/ThrK, serine/threonine kinase; STAS, sulfate transporter anti-s antagonist; HTH, helix−turn−helix. (C) Schematic of light-induced cysteinyl−FMN (C4a) covalent adduct formation. (D) Genetic context of the LOV domain protein in *R. sphaeroides*.

second mode of dimerization, with intermolecular contacts primarily in the Ncaps, while YtvA utilizes both modes of dimerization, using contacts in the β-scaffold and in the C-terminal extension (Jα helix) to form a dimer (Figure 3).[36] Structurally characterized tandem PAS structures have head-to-tail PAS-A to PAS-B associations that form parallel or antiparallel dimers mediated by extensive contacts between exposed β-sheet and α-helical extensions.[37,38]

R. sphaeroides is a purple photosynthetic Gram-negative bacterium (α-proteobacterium) that contains a short LOV domain protein in addition to other light-sensing proteins that include AppA, a blue-light-sensing FAD photoreceptor, and three cryptochrome-like proteins.[39,40] The LOV domain protein of *R. sphaeroides* (RsLOV) binds flavin mononucleotide (FMN) as its chromophore. RsLOV is 18% identical to *N. crassa* VVD, with a moderate pairwise score of 25.[41] Sequence alignments of RsLOV and VVD reveal structural similarities in the LOV core region, but differences in the terminal extensions (Figure 1A). Specifically, the N-terminal latch of VVD, which participates in a "domain swapping" interaction to allow VVD light-dependent dimerization,[19] is lacking in RsLOV; however, the receptor pocket for the VVD N-terminal latch is conserved. RsLOV also contains a C-terminal extension absent in VVD but present in YtvA and the LOV2 domain of *Avena sativa* (oat, AsLOV2),[42] which have pairwise scores from ClustalW of 28 and 25, respectively.[43,44] Other LOV domain proteins with similar sequences include the LOV proteins from *P. putida* (soil bacterium, PpSB1-LOV)[45,46] and *Erythrobacter litoralis* (marine bacterium, EL222). PpSB1-LOV has an N-terminal extension similar in length to that of RsLOV and a C-terminal Jα helix shorter than that of RsLOV,[45] whereas the LOV domain protein from EL222 has a short N-terminal extension and a Jα helix that attaches to a helix−turn−helix (HTH) effector domain.[47]

The differences in LOV domain light-dependent signaling processes are exemplified by the structural changes induced in LOV proteins VVD, YtvA, and AsLOV2 upon their exposure to light. VVD forms a light-induced dimer through an N-terminal helix and flexible coiled regions.[19−22] YtvA exhibits a light-induced rotation of subunits in its head-to-head dimer that involve changes in intermolecular contacts between the C-terminal Jα helices and between the individual β-scaffolds.[17,48,49] In the isolated AsLOV2 domain of plant phototropin, light-induced rearrangements of hydrogen bonds within the structural core propagate to changes in both the N- and C-terminal flanking regions that result in a partial unfolding

dx.doi.org/10.1021/bi3015373 | *Biochemistry* 2013, 52, 378−391

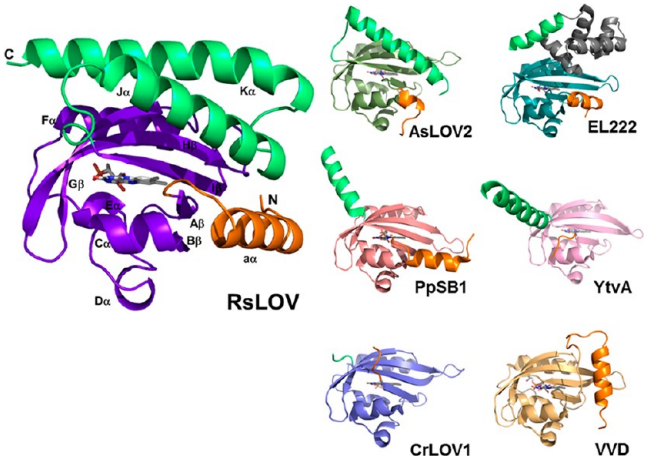

Figure 2. LOV subunit structures. RsLOV structure in the dark state, with the PAS core colored violet, the N-terminal extension orange, and the C-terminal extension light green. Dark-state structures of *N. crassa* VVD (2PD7, PAS core colored light orange), *Avena sativa* LOV2 (2V1A, PAS core colored forest green), *C. reinhardtii* LOV1 (1N9L, PAS core colored light blue), *B. subtilis* LOV (2PR5, PAS core colored pink), EL222 (3P7N, PAS core colored aqua, HTH motif colored gray), and *P. putida* (3SW1, PAS core colored salmon), with N-terminal extensions colored orange and C-terminal extensions light green.

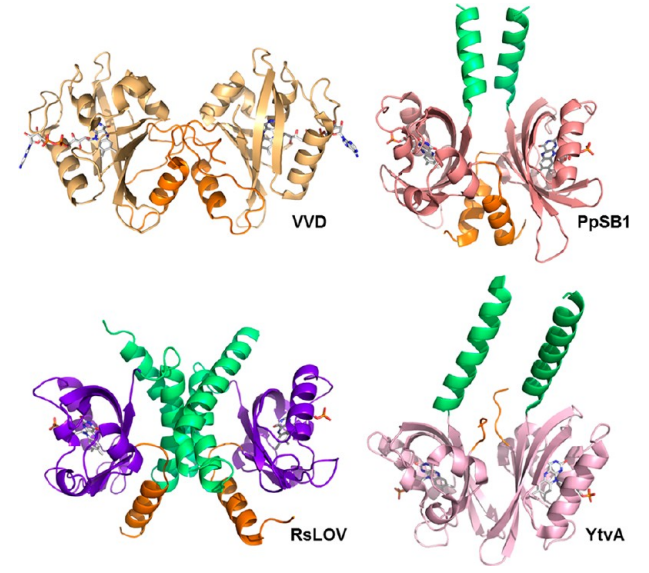

Figure 3. Comparison of LOV dimers. Light-state structure of *N. crassa* VVD (3RH8, light orange), dark-state structure of *B. subtilis* LOV (2PR5, pink), light-state structure of *P. putida* (3SW1, salmon), and dark-state structure of RsLOV (purple), with N-terminal extensions colored orange and C-terminal extensions light green.

of the Jα helix, but the protein does not homodimerize.[17,31,50] However, the proteins display conserved aspects of signal propagation from the flavin chromophore to the variable peripheral elements despite differences in light-induced conformational changes in these peripheral regions.[4]

The LOV protein of *R. sphaeroides* ATCC 17025 is a short LOV (*rsp*2265) lacking an effector domain. Downstream on the chromosome from the RsLOV gene is a large 1165-amino acid protein that contains PAS, histidine kinase, *S*-adenosylmethionine methyltransferase, CheR methyltransferase, and CheB methylesterase domains [*rsp*2264 (Figure 1D)]. Upstream of RsLOV are a hypothetical protein of 224 residues (*rsp*2268) and a 409-amino acid glycogen-1-phosphate adenylyltransferase (*rsp*2266). Previous studies of RsLOV from a similar *R. sphaeroides* strain implicated the protein in photosynthetic gene expression in a manner similar to that of the other two photoreceptor proteins of *R. sphaeroides*, AppA and CryB.[51] Thus, functional and gene clustering analyses potentially involve RsLOV function in carbohydrate metabolism, chemotaxis, and cellular response to photooxidative stress.

Herein, we investigate the molecular mechanism behind the light-dependent signaling of RsLOV, specifically, how the photosensor protein generates and propagates light absorption to changes in protein conformation and association. Through a combination of crystallographic and biochemical studies, we define the structural features of RsLOV and describe how flavin photochemistry correlates to changes in the oligomeric state of the protein.

MATERIALS AND METHODS

Protein Expression and Purification. The RsLOV (*R. sphaeroides* 17025) gene was cloned into expression vector pET28a (Novagen) in frame with an N-terminal His tag using *Nde*I and *Endo*RI restriction sites. Site-directed mutagenesis by overlap extension with the polymerase chain reaction generated point mutation constructs of RsLOV: T21V, L32V, C55A, I71L, I71V, L101I, S127C, A136C, A136Y, A138Y, E142C, R145C, and A167C. All were cloned between *Nde*I and *Endo*RI restriction sites and sequenced in their entirety at the Biotechnology Resource Center of Cornell University.

RsLOV constructs were overexpressed in *Escherichia coli* BL21(DE3) cells. Cultures were induced with 100 μM IPTG at a cell density (OD_{600}) of 0.6−0.8. Proteins were expressed for 20−22 h at 17 °C and shaken at 170 rpm under constant light. Cells were harvested by centrifugation (8000 rpm and 4 °C for 15 min) and flash-frozen in liquid N_2, and the cell pellets were stored at −80 °C. Cell pellets were resuspended in buffer containing 50 mM Tris (pH 8.5), 10 mM imidazole, and 300 mM NaCl and lysed by sonication, and cell debris was subsequently removed by centrifugation (22000 rpm and 4 °C for 1 h). The soluble cell lysate was purified with Ni-NTA affinity chromatography. The eluted protein was concentrated and treated with thrombin overnight. Samples were then purified on a Superdex 75 Hi-load 26/60 fast performance liquid chromatography (FPLC) column and concentrated to 5−30 mg/mL by centrifugation. Analytical size exclusion chromatography (SEC) FPLC was completed using a Superdex 200 10/300 analytical column. The column was equilibrated with buffer containing 150 mM NaCl and 50 mM Tris (pH 8.5). Samples were injected in 500 mL aliquots and run at a flow rate of 0.3 mL/min.

Crystallization, Data Collection, and Structure Determination. Orthorhombic RsLOV crystals in space group $P2_12_12_1$ and hexagonal RsLOV crystals in space group $P6_5$ were obtained at 17 °C under constant darkness by vapor diffusion. Crystals grew from an equal volume (1.5 μL) of 30 mg/mL protein in buffer containing 50 mM Tris (pH 8.5) and 150 mM NaCl and the reservoir solution: 30% PEG 400, 0.15 M $MgCl_2{\cdot}6H_2O$, 0.1 M HEPES (pH 8.5) (orthorhombic) or 0.1 M HEPES (pH 7.5), and 4.3 M NaCl (hexagonal). RsLOV crystallizes as single rods, which diffract to ∼2.4 Å resolution. L32V RsLOV crystals in space group $P2_12_12_1$ grew from $LiSO_4$ in 0.1 M HEPES (pH 7.9) and diffract to 1.9 Å resolution. A138Y RsLOV crystals in space group $P6_5$ grew from 0.1 M

dx.doi.org/10.1021/bi3015373 | *Biochemistry* 2013, 52, 378−391

HEPES (pH 7.5) and 4.3 M NaCl and diffract to 2.6 Å resolution. Data were collected at 100 K on beamlines A1 and F1 at the Cornell High Energy Synchrotron Source (CHESS). Dark-state crystals were excited to the light state by white-light illumination while still in solution prior to being cryo-cooled to 100 K. To minimize reduction of the covalent adduct formed in the light-adapted protein by the X-ray beam, two strategies were employed to stabilize the adduct as reported previously.[19,21] To reduce radiation exposure, each frame was collected over a 1−5° oscillation per second (X-ray flux of 3×10^{11} photons/s per 0.2 mm × 2.00 mm focus at 0.979 Å), and secondly, data were collected from several different spots on a single crystal and then merged with data collected on additional crystals in the same manner, to generate the complete data set. Data were reduced and scaled using HKL2000.[52] Initial phases were determined by molecular replacement in AutoMR (Phenix)[53] using VVD (Protein Data Bank entry 2PD7[21]) as a search model. Models were rebuilt and fit using XFIT[54] followed by refinement using CNS[50] (Table S1 of the Supporting Information) and Phenix.[55]

SAXS Data Collection and Analysis. SAXS data were collected at beamline F2 at the CHESS at 9.881 keV. RsLOV solutions at concentrations of 2.5, 5, and 10 mg/mL in a buffer consisting of 2 mM DTT, 1% glycerol, 50 mM Tris (pH 8), and 150 mM NaCl were used for the SAXS analysis. The X-ray beam was collimated to 250 mm × 250 mm and was centered on a 2 mm diameter vertical quartz capillary tube with 10 mm thick walls (Hampton Research, Aliso Viejo, CA). The protein samples were centrifuged at 14000 rpm for 10 min prior to data collection. Sample aliquots of approximately 15−20 μL were delivered from a 96-well plate to the capillary using a Hudson SOLO single-channel pipetting robot (Hudson Robotics Inc., Springfield, NJ). To reduce the extent of radiation damage, the sample plugs were oscillated in the X-ray beam using a computer-controlled syringe pump (Aurora Biomed, Vancouver, BC). Images were collected on a Quantum 1 CCD detector (Area Detector Systems Corp., Poway, CA) with six sequential 30 s exposures being used to assess possible radiation damage. Dark samples were wrapped in aluminum foil until they were placed in the 96-well plate to minimize light activation. Light samples were exposed to white light prior to addition to the plate, and data collection was initiated within a short time (seconds to minutes) to minimize the contribution from the recovered dark-state sample.

Scattering data were processed according to previously described protocols[56] utilizing BioXTAS RAW,[57] and programs from the ATSAS[58−60] and SITUS[61] packages. SAXS of hen egg white lysozyme (MW = 14700 Da) and glucose isomerase (MW = 173000 Da) were collected as references for determining the apparent MW of RsLOV. Additionally, the SAXS MoW tool developed by Fischer et al.[62] was applied to the data for MW calculations. The MW values derived from SAXS MoW utilizing the GNOM output files are reported herein (Table S3 of the Supporting Information). Fits to the experimental SAXS data were generated using CRYSOL[63] and a combination of RANCH13 and GAJOE13 for the EOM approximations.[64] In the CRYSOL fits, the dimer model was the $P6_5$ dark-state structure and the monomer model was chain A from the $P6_5$ dark-state structure. In the EOM approximation, the monomer model included residues 20−125 of $P6_5$ dark-state structure chain B as the folded domain, whereas the rest of the chain was treated as random coil; the dimer model included residues 5 (chain A) through 172 (chain B) as the folded domain, while the remaining residues were treated as random coil. Envelopes were generated using the output of DAMFILT preceded by DAMAVER[65] completed with 10 DAMMIF[66] calculated reconstructions, as input for the pdb2vol utility in the SITUS package. A rigid body search to fit crystallographic models into SAXS envelopes was completed using the COLLAGE utility in the SITUS package.

Light Scattering. Multiangle light scattering (MALS) was conducted on RsLOV with a Protein Solutions Dynapro dynamic light scattering instrument over a concentration range of 100−500 μM. Dark- and light-state samples were injected into a Sephadex 75 10/300 analytical column, which was connected to a Wyatt miniDAWN Treos multiangle light scattering system. Absolute MW calculations were completed using ASTRA version 5.0 from Wyatt Technologies.

Cross-Linking. Cross-linking studies of RsLOV variants with cysteine residues introduced at positions 127, 129, 136, 138, 142, and 145 were conducted under native and oxidizing conditions. For oxidizing conditions, cross-linking was induced via the addition of 0.5 mM Cu(II)(1,10-phenanthroline)$_3$ to dark- and light-state protein samples at concentrations of 4−8 mg/mL. Changes in oligomerization were assessed by sodium dodecyl sulfate−polyacrylamide gel electrophoresis and analytical SEC FPLC.

Time-Resolved Absorption Spectroscopy. Time-resolved electronic absorption spectroscopy measurements of RsLOV and RsLOV mutants were performed using an Agilent 8453 spectrophotometer. Samples were excited to the light state using white light from a Xe arc lamp. Measurements of dark-state recovery rates were taken every 30 s for 2−4 h. Absorbance traces at 450 and 310 nm were fit assuming first-order kinetics with a single rate constant, using a mono-exponential function ($\text{Abs} = B + Ce^{-kt}$). Average rate constants were determined from multiple measurements.

Accesion Codes. The crystal structures of RsLOV in the dark-adapted ($P2_12_12_1$ and $P6_5$) and light-adapted states, L32V RsLOV, and A138Y RsLOV in the dark state were deposited as Protein Data Bank entries 4HJ4, 4HJ6, 4HNB, 4HIA, and 4HJ3, respectively.

RESULTS

Dark State of RsLOV. Orthorhombic crystals of RsLOV that were grown in the dark diffracted to 2.4 Å resolution (Table S1 of the Supporting Information) at the synchrotron. The crystallographic structure was determined by molecular replacement using dark-state VVD (PDB entry 2PD7) as the probe. The two molecules of RsLOV in the asymmetric unit form a tight dimer that is related by noncrystallographic symmetry. RsLOV adopts the PAS fold[1] with the conserved core of a five-stranded antiparallel β-sheet, Aβ (Leu20−Met25), Bβ (Pro31−Ala35), Gβ (Glu80−Arg89), Hβ (Glu93−Gly106), and Iβ (Pro111−Leu121), and helical connector elements Cα (Pro37−Thr43), Dα (Glu47−Gly52), Eα (Cys55−Gln59), and Fα (Ala65−Leu77).

Auxiliary to the PAS core, RsLOV has an additional N-terminal aα helix (Met1−Arg15) and a C-terminal helix−turn−helix motif composed of helices Jα (Glu128−Ile146) and Kα (Leu153−Gly176) (Figure 2). The 15-residue N-terminal helix (aα) is 21 Å in length and attaches to Aβ through a short five-residue loop that includes Gly17 in the hinge. The aα helix is adjacent to the end of the Jα helix and flanks the β-scaffold for most of its length until the Hβ−Iβ loop is reached. The aα helix is amphipathic; the solvent-exposed side of the helix consists of

dx.doi.org/10.1021/bi3015373 | Biochemistry 2013, 52, 378−391

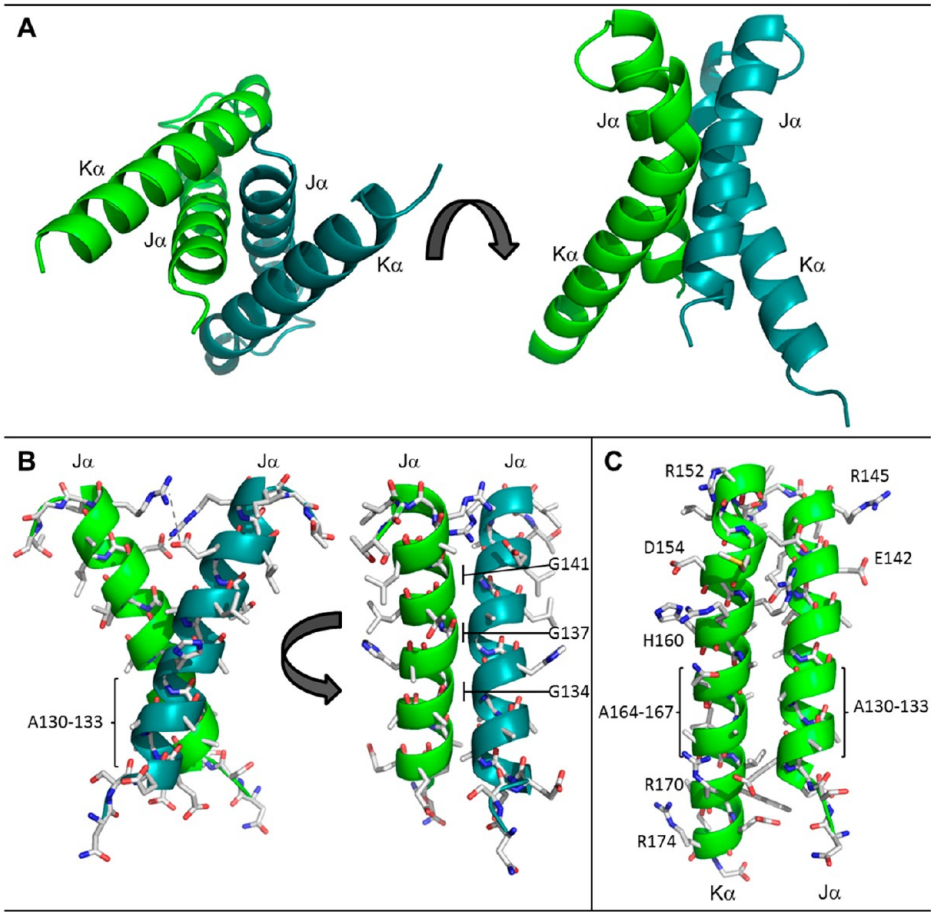

Figure 4. RsLOV dimerization motif. (A) Four-helix bundle at the interface of the RsLOV crystallographic dimer, with subunits A and B distinguished by color. (B) Side chain contacts at the helix Jα interface of chain A and chain B. (C) Side chain contacts at the helix Jα–helix Kα interface. There are salt bridges between Arg145 and Glu142 (same monomer) and between Arg15 and Glu154 (opposing monomer). Hydrogen bonding interactions range from 2.45 to 3.66 Å in length, including those from the amide H of Arg158 to the backbone O of Gly17 (opposing monomer) and from the amide H of Arg159 to the side chain O of Ser124 (opposing monomer). The residues with the most buried surface area are within the crossing point of the two Jα helices at the region of the four-alanine repeat: Ala130–133, Gly134, Gly137, Ala138, and the cross section of Kα, including Glu154, Arg158, and Ala162.

hydrophilic and charged residues, whereas the inner side that flanks the β-sheet is generally hydrophobic. Asn36 mediates a direct interaction between the aα helix and Bβ.

The C-terminal helix–turn–helix motif composes the dimer interface from roughly 48 residues on each subunit. The shorter Jα helix is 29 Å in length, whereas the longer Kα helix extends 40 Å. The helices are at an ~30° angle to one another and make a close central crossing of 3.8 Å in the region of Ala136, Ala162, Thr140 and Arg158, and Val169 and Glu129. The proximity of the helices is largely due to four-alanine repeat sequences at their centers and several glycine residues (Figures 1 and 4). His135 anchors the Jα helix to the LOV domain via Iβ Ser117. The Jα–β-scaffold interface is primarily hydrophobic, with Jα helix nonpolar residues Ala132, Leu139, Leu143, and Ile146 extended toward the sheet and the nonpolar side chains of Leu115 and Phe119 of Iβ extended toward the helix. Direct interactions between helices Jα and aα occur via hydrogen bonding residues Arg15 and/or Ser16 and Glu142. The Kα helix has Leu161, Leu168, and Trp172 directed toward the β-sheet, whereas Hβ has Leu98 and Phe100 directed toward the Kα helices.

RsLOV is unique among short LOVs in that it has both N- and C-terminal flanking helices that could interact with an effector protein. At the center of the crystallized dimer interface are the C-terminal helix–turn–helix motifs (helices Jα and Kα) of the two subunits (A and B) that pack against each other in a coiled coil to form a distorted four-helix bundle with a highly unusual packing interface. The Jα–Kα helix dimer interface has a highly complementary solvent exclusive core formed primarily by close symmetric interactions of three helix Jα Gly residues (134, 137, and 141) that allow the 137–138 peptide bonds from each subunit to stack against each other (~3.5 Å). Packing of the Ala_4 repeats at the beginning of helix Jα (residues 130–133) and the end of helix Kα (residues 162–167) in roughly perpendicular helices also mediates an especially tight interface (Figure 4). Long side chains at the ends of the helices stabilize the periphery of the interface with salt bridges and hydrogen bonds. In total, the dimer interface involves 34 residues and buries 1100 $Å^2$ per subunit but because of the predominance of Ala and Gly residues does not contain the branched hydrophobic side chains typical of coiled coils. As a result, interface analysis as performed with PISA complex[67,68] indicates that the contact buries a small amount of hydrophobic surface area (ΔG of complex formation of −0.4 kcal/mol) and therefore is unlikely to participate in solution dimerization. However, this estimate is based almost exclusively on buried hydrophobic surface area, and there are also substantial hydrophilic interactions between the subunits, including salt

dx.doi.org/10.1021/bi3015373 | *Biochemistry* 2013, 52, 378–391

bridges between Arg145 and Glu142 and between Arg15 and Glu154. This, and the unusual packing interactions at the bundle core mediated by the symmetric contacts of the Gly and Ala repeats, suggests that the dimer interface may not simply be a result of crystallization.

The FMN binding pocket buries the isoalloxazine ring in the β-scaffold and exposes the ribityl phosphate chain to solvent. The pocket is polar on the pyrimidine side of the isoalloxazine ring where its closest contacts are those with Gln59, Asn87, and Asn97; nonpolar around the dimethylbenzimidazole moiety with proximal residues Val23 and Phe114; and polar along the solvent-exposed ribityl phosphate where the phosphate interacts with Arg56 and Arg68. The S atom of Cys55 is 4.5 Å from C4a of the FMN in the dark state. At the periphery of the LOV domain, Arg56, Arg68, Gln29, and Gln59 interact with the FMN phosphate moiety, and inside the pocket, Asn87 and Asn97 form hydrogen bonds to the pyrimidine ring of the flavin.

Light State of RsLOV. Illumination of RsLOV in solution generates a distinct photobleaching of the protein associated with formation of the cysteinyl–flavin adduct. This is seen by a change from the dark-state absorption peak at 447 nm to the maximal light-state absorption peak centered at 390 nm (Figure 5B). As part of the reversible photocycle, the cysteinyl–flavin adduct (S_{Cys55}–C4a) spontaneously breaks down in a first-order reaction with a lifetime of 2357 s.

To investigate changes in structure induced by light exposure, crystals were irradiated with white light until they were visibly bleached and then flash-frozen. It is well-known that the adduct is not stable to the reducing power of the synchrotron beam,[19,21,69] and thus, the light-state data set was composed from data collected on multiple crystals that were each minimally exposed. In the final 2.14 Å resolution structure, the flavin–cysteinyl adduct is present in only one subunit of the RsLOV crystallographic dimer, and even in that one subunit, the light state is not fully occupied, with approximately 40% of the molecules present in an alternative (dark state) conformation. In the light-state structure, the Cys–FMN adduct forms with a S_{Cys55}–C4a bond distance of ~1.8 Å. The planarity of the reduced FMN is disrupted, with C4a pulled up above the ring plane and N5 and O forced below the plane by the S_{Cys55}–C4a bond. This effectively breaks the conjugated π-system and induces a pucker across the isoalloxazine ring (Figure 6A). In general, the dark- and light-state structures have very similar conformations. This is not surprising because the conversion of RsLOV to the light state within the confines of the dark-state crystals likely eliminates the possibility of large-scale conformational changes. Nonetheless, light minus dark ($F_L - F_D$) Fourier difference maps identify residues that exhibit some perturbation in position or dynamics from dark to light state (Figure 6C). Residues that show difference peaks of $\geq 3.5\sigma$ are primarily within the first sphere of the flavin, on the interior of the binding pocket; these include Thr21, Leu22, Val23, Met25, Cys55, Phe100, Leu115, and Gln118 (Figure 6B). It appears that conformational changes propagate from FMN N5, which will undergo protonation upon adduct formation, through the β-sheet, to proximal second-sphere residues, including Leu34, Leu51, Phe13, and Arg10. Arg10 and Phe13 are residues in the N-terminal flanking helix. The largest light–dark residue changes are observed at Ala133 and Gln49. Ala133 resides in the center of the Jα helix, whereas Gln49 is in the Dα helix, a solvent-exposed structural feature on the periphery of the domain. The potential of signal propagation through to the Jα helix has been shown before in the AsLOV2 protein.[70,71] Our data also indicate that the unique flanking terminal regions of RsLOV respond to adduct formation and that a series of conformational changes, dampened by the crystal lattice, propagate from the N5 edge of the flavin, through Iβ, to the terminal helices at the dimer interface.

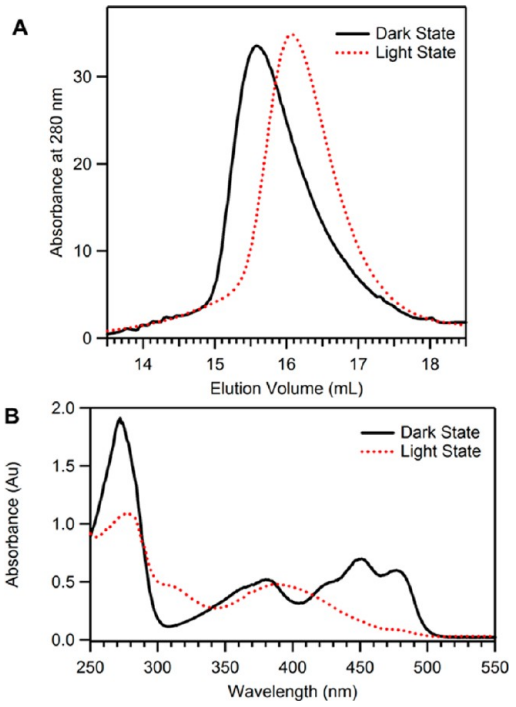

Figure 5. Solution properties of RsLOV. (A) Elution profile of RsLOV expressed in *E. coli* with a Superdex 75 10/300 column. The light state (red dotted line) elutes at 16.1 mL and the dark state (black solid line) at 15.5 mL. (B) Electronic absorption spectra of light-state RsLOV (red dotted line) and dark-state RsLOV (black solid line).

In VVD, the conserved Gln residue in the Iβ sheet (Gln182 in VVD and Gln118 in RsLOV) flips upon blue-light excitation and thereby alters hydrogen bonding interactions with the backbone of Ala72, which precedes the Aβ strand in the hinge region of the N-terminal helical cap.[19,21] Thus, in VVD, the hinge region between the Ncap and PAS β-sheet plays a major role in mediating light-activated conformational changes between the flavin center and the protein interaction regions.[19] The reorientation of the Gln residue and its role in disrupting hydrogen bonding interactions that extend to the surface of the protein have also been supported in LOV2, LOV2-Jα, and full-length phototropin systems.[71−75] Although the Ala72 residue that couples to the N-terminal cap in VVD is conserved in RsLOV (Ala19), differences in the neighboring residues, especially the presence of Thr21 in RsLOV, suggest that the mechanism of conformational propagation may not be conserved. The side chain hydroxyl group of Thr21 is closer to the Gln118 residue (3.4 Å) than the carbonyl O of Ala19 (3.8 Å) (Figure 6B). In AsLOV2, changes in hydrogen bonding triggered by a conformational change in flavin-interacting Gln513 strengthen the coupling between the Iβ and Hβ strands. This overall tightening of the β-sheet leads to detachment of the Jα helix from its outside surface.[71] In AsLOV2, Asn482 and Asn492 hydrogen bond with the flavin and Gln513. Changes in the dynamics of these residues upon

dx.doi.org/10.1021/bi3015373 | *Biochemistry* 2013, 52, 378−391

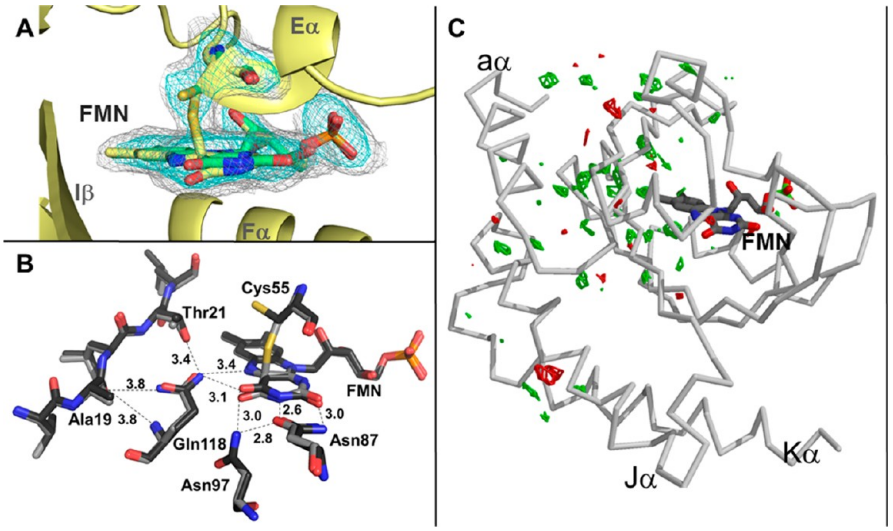

Figure 6. Irradiation of RsLOV crystals. (A) Light-state structure of RsLOV with electron density corresponding to the light-induced cysteinyl−C4a adduct of Cys55 and FMN [$F_o - F_c$ simulated annealing omit map, obtained by omitting the flavin molecule and Cys55 residue, contoured at 2.2σ (cyan) or 0.7σ (gray)]. The two conformations of Cys55B and flavin are colored yellow (covalently bound) and green (unbound). (B) FMN binding pocket residues affected by changes in light-state conversion. (C) RsLOV structure in the light state with an $F_o - F_o$ difference map of light−dark amplitudes (green for 3.5σ and red for −3.5σ).

adduct formation are thought to be critical for propagating a light signal to the surface of the protein.[71] Both residues are conserved in RsLOV (Asn87 and Asn97, respectively). Because RsLOV has both aα and Jα/Kα extensions, it is possible that a hybrid form of these aforementioned structural changes is responsible for propagating conformational changes out from the flavin. The hinge region is likely to be affected by N5 protonation and Gln rearrangement, as is the association of helix Jα with the PAS β-sheet. Although the crystal lattice prevents observation of large-amplitude perturbations, the difference Fourier analysis does anticipate conformational changes in all of these regions.

Solution-State Behavior of RsLOV. RsLOV elutes via SEC at a MW consistent with a dimer. To test whether the RsLOV solution dimer is the same as that observed in the crystal, we engineered Cys residues at the dimer interface and evaluated their ability to cross-link. Cys residues placed on helices Jα and Kα cross-link the subunits effectively, even in the absence of oxidants, confirming that the crystallographic dimer is represented in solution (Figure 7B, Figure S3 of the Supporting Information, and Table 1). Moreover, mutation of E142, which participates in a salt bridge with Arg145 of the opposing subunit, completely abolished dimerization in the dark (Figure 4B and Figure S3 of the Supporting Information). Thus, RsLOV dimerizes through the interface found in the crystals.

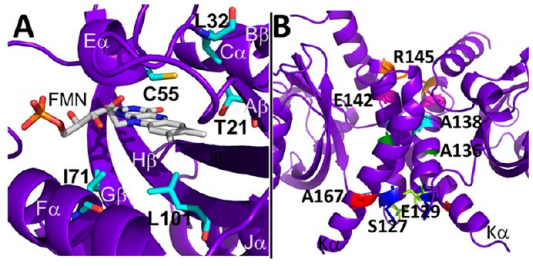

Figure 7. RsLOV point mutants. (A) Dark-state structure of RsLOV with residues adjacent to the FMN binding pocket targeted for point mutations colored cyan. (B) Residues targeted for point mutations at the RsLOV dimer interface highlighted: S127 (yellow), E129 (blue), A136 (green), A138 (aqua), E142 (pink), R145 (orange), and A167 (red).

Table 1. Results of Cross-Linking in RsLOV Variants Showing the Distances between Cα Atoms in the Relevant Cys Residues, the *B* Factors of the Cys Cα Atoms, the Oligomeric State in the Dark, and Whether the Level of Cross-Linking Increases upon Addition of Cu(phen)$_3$ in the Dark[a]

variant	distance between Cα atoms (Å)	*B* factor of Cα	dimer or monomer in the dark	cross-linked by Cu(phen)$_3$ in the dark
wild type (C55)	48.2	47.8	monomer	no
S127C	14.3	66.4	dimer/ monomer	yes
A136C	10.1	37.7	monomer	yes
E142C	10.1	46.6	monomer	no
R145C	11.3	56.0	monomer/ dimer	no
A167C	17.9	55.1	dimer/ monomer	yes

[a]The gel is shown in Figure S3 of the Supporting Information.

Upon conversion to the adduct state, RsLOV elutes at a much later volume on SEC compared to the dark state (Figure 5A and Figure S2 of the Supporting Information).[39] The transparent column was exposed to white light for the duration of the SEC experiments to minimize dark-state reversion, which occurs with a half-life of 27 min. The elution profiles of the light state are consistently shifted by ~0.6 mL, which corresponds to an 8.3 kDa reduction in MW. This is not enough of a MW shift for a full dimer to monomer conversion (which would represent a change of ~19 kDa), but the reduction in the light-state elution volume was consistent across a large range of protein concentrations. The oligomeric state of RsLOV was further analyzed by multiangle light scattering (MALS). In the case of SEC-coupled MALS, the protein could not be irradiated

dx.doi.org/10.1021/bi3015373 | *Biochemistry* 2013, 52, 378−391

during chromatography, which typically took ~40 min to complete. Nevertheless, the light state consistently showed a smaller MW than the dark state. In fact, the MALS-determined light-state MW (20.4 kDa) was very close to that predicted for a pure monomer (19.9 kDa), whereas the dark-state MW was smaller (30.2 kDa) than that predicted for a true dimer (39.8 kDa) (Figure S1 and Table S2 of the Supporting Information). The behavior of the dark state is consistent with a dimeric species that exchanges rapidly with a monomeric species on the time scale of size exclusion,[20] and thus, the MALS data support a monomer−dimer equilibrium that is shifted toward the monomer by light.

Small-angle X-ray scattering was also used to determine the oligomeric state of RsLOV in both the light and dark states. In total, from the time of light exposure, the experiment took less than 10 min for complete data collection, allowing only minimal dark-state recovery. The molecular weights derived from SAXS MoW analysis of GNOM output files[76,77] of the experimental SAXS data predict a dark-state MW of 34.1 kDa and a light-state MW of 27.8 kDa, which is higher than that of the smaller species observed via MALS. This is probably explained by the fact that protein concentrations used for SAXS are higher than that found on the MALS SEC column and thus favor some dimerization of the light state. It is also possible that the synchrotron beam reduces the adduct to some extent and drives the system back toward a dimer. Theoretical scattering curves for the crystallographic dimer and monomer structures were generated and fit to the dark- and light-state experimental SAXS data using CRYSOL[63](Figure 9A,B). The theoretical curve generated for the dimer structure fits well to the dark-state experimental data (χ^2 value of 0.9). The theoretical curve generated for an RsLOV monomer does not fit either state well, χ^2 values of 3.5 (dark) and 2.6 (light) indicating some contribution from dimer and possibly conformational changes in the monomer that are not modeled well using the single compact subunit of the RsLOV crystal structure. The best fit to the light-state experimental data was obtained using the ensemble optimization method (EOM) via RANCH and GAJOE[64] with a monomeric model made from an ordered LOV domain core and disordered N-terminal aα helix and the C-terminal Jα and Kα helices (χ^2 value of 0.42). However, the predicted molecular weight derived from this experimental SAXS data indicates a contribution from an RsLOV dimer even in the "light-state" ensemble. Accordingly, the best fit to the experimental scattering curve came from a linear combination of calculated scattering from the EOM-modeled monomer and the CRYSOL-predicted dimeric state (Figure 9B). In further support of an altered monomer structure, Kratky plots of the SAXS data, which emphasize changes at larger q values (i.e., intramolecular), are indicative of a more unfolded light state (Figure 9C). The ~1 Å difference in experimental R_g values between the dark and light state at three protein concentrations (Table S3 of the Supporting Information) agrees well with the difference between average R_g values from the EOM models of the monomer and dimer with varying degrees of disorder (21.9 and 22.6 Å, respectively). These slightly larger values, compared to those predicted from CRYSOL with the static crystal structures, (17.9 Å for the monomer and 21.4 Å for the dimer), support enhanced flexibility in the light state, and perhaps in the dark state to a lesser extent. The predicted molecular envelopes based on the SAXS (Figure 9D, corresponding data, and Table S3 of the Supporting Information) confirm that the dark-state envelope completely overlays the crystallographic dimer, whereas the light state fits a monomer with additional, unfilled volume. The unfilled volume in the light-state envelope could result from a monomer with terminal helices in an extended conformation and/or a contribution from the dimeric state. Although the fits to the scattering curves themselves are the most reliable indicators of the light-state ensemble, the envelope reconstructions do reflect what we believe to be the key changes upon conversion of RsLOV to the light state: loss of dimer content and increase in the level of subunit disorder.

Variants of RsLOV That Affect Dark-State Recovery. Sequence variations in LOV proteins and related PAS domain proteins like PYP have been shown to alter thermal reversion rates and affect overall protein stability.[22,78,79] In previous studies of LOV domain variants, substitutions that affected hydrophobicity, solvent accessibility, hydrogen bonding, and salt bridges in the flavin pocket all altered adduct lifetime. In RsLOV, we examined active site variants Thr21 → Val, Leu32 → Val, Ile71 → Leu, Ile71 → Val, Leu101 → Ile, and Cys55 → Ala, which were all chosen to alter the adduct-state stability. Cys55 forms the adduct state with the C4a atom of FMN. Indeed, UV−vis spectroscopy confirmed that the Cys55 → Ala variant does not form the light-state adduct. Thr21 (5 Å to Cys55, 3.6 Å to FMN C6) and Leu32 (3.3 Å to Cys55) were expected to affect the conformational stability and solvent accessibility of Cys55. Ile71 (3.7 Å to O3′ in FMN tail) and Leu101 (3.8 Å to FMN C7) contact the *re* face of the flavin ring and influence solvent access in the FMN binding pocket (Figure 7A).

Despite the relatively conservative residue substitutions, each variant decreased the adduct stability (Table 2). The substitution at Leu32 had the most substantial increase in thermal revision rate, which increased 14-fold in the variant. Substitutions at Thr21, Ile71, and Leu101 also increased the thermal reversion rate, though to a lesser extent, ~1.4−3-fold. None of the FMN binding site variants decreased the reversion rate.

Table 2. Parameters for Adduct Decay Kinetics in RsLOV Variants and Comparable LOV Domain Proteins

variant	rate constant (s^{-1})	lifetime (s)
RsLOV	4.2×10^{-4}	2374 ± 304
T21V	1.3×10^{-3}	799 ± 78
L32V	6.1×10^{-3}	164 ± 7
I71L	5.6×10^{-4}	1801 ± 362
I71V	6.5×10^{-4}	1544 ± 95
L101I	6.1×10^{-4}	1647 ± 71
S127C	6.5×10^{-4}	1536 ± 122
E142C	5.3×10^{-4}	1904 ± 99
A167C	5.8×10^{-4}	1720 ± 162
R145C	3.5×10^{-4}	2849 ± 268
A136C	3.9×10^{-4}	2587 ± 96
A136Y	4.2×10^{-4}	2372 ± 802
A138Y	5.5×10^{-4}	1829 ± 62
wild-type (WT) YtvA[a]	2.8×10^{-4}	3600
WT AsLOV2[a]	1.2×10^{-2}	81
VVD-36[a]	5.6×10^{-5}	18000

[a]Values obtained from ref 22.

Leu32 resides on the bβ strand proximal to the flexible connective loop region within the FMN binding pocket and is within van der Waals contact distance of Cys55 (3.3 Å). Substitution of Leu with Val would increase the volume of the

dx.doi.org/10.1021/bi3015373 | *Biochemistry* 2013, 52, 378−391

pocket, make additional space for solvent, and disrupt the packing of Cys55. Because the most substantial changes to thermal reversion rate were caused by the Leu32 → Val mutation, we further characterized this substitution by determining the L32V dark-state crystal structure (vide infra).

The changes in recovery rate exhibited by the remaining variants, at Thr21, Ile71, and Leu101, are modest, although their structural contexts provide possible explanations for the slightly increased recovery rates. In VVD, thermal reversion is rate-limited by deprotonation of N5;[22] thus, changes that increase the solvent accessibility of the pocket are likely to destabilize the adduct. Thr21 contacts hydrogen bonds from FMN C6 to the conserved Gln118 and resides within the first sphere of residues adjacent to Cys55. The change from Thr21 to Val will eliminate hydrogen bonding interactions through the side chain and introduce more nonpolar character into the binding pocket. Ile71 and Leu101 are situated below the *re* face of FMN, and changes in these residues would be expected to affect the access of the solvent to flavin N5 and likely the flavin redox potential.[19,22] Ile71 is on the interior of Fα and within 4 Å of the FMN ribose moiety, and Leu101 is on the Hβ strand. For both positions, removal or addition of a methyl group is likely to subtly alter the accessibility, dynamics, and redox properties of the adduct, thereby producing the small reductions in light-state stability that were observed.

The variants that introduced Cys and Tyr residues into the C-terminal helices were also analyzed for effects on light-cycle kinetics (Figure 7B). Like most variants proximal to the FMN binding site, the variants in the Jα and Kα helices had a minimal effect on the reversion rates. The largest deviations from that of the WT were R145C, with a 1.2-fold longer recovery, and S127C, with a 1.6-fold shorter recovery.

Structure of the L32V RsLOV Variant. To further investigate the 14-fold change in recovery rate caused by the Leu32Val substitution, orthorhombic crystals of RsLOV L32V were grown. Interestingly, crystal growth required conditions different from those used for wild-type RsLOV, and the resulting cell dimensions were also different from those of the wild-type crystals. Data were collected from a single crystal to 1.9 Å resolution and scaled in the $P2_12_12_1$ space group, and the structure was determined by molecular replacement with WT RsLOV as a probe (Table S1 of the Supporting Information). Leu32 is found on Bβ, approximately 3.3 Å from the Cys55 residue. The most substantial differences in electron density due to the Val mutation are located in three of the four consecutive helices on the *si* face of the flavin: Dα, Eα, Fα, and the flexible loops that connect them (Figure 8A). The turn that connects Aβ and Bβ sheets and the loop that connects Eα and Fα helices are all repositioned with respect to the WT RsLOV structure. The alterations in loop position correlate with increased *B* factors in these regions (Figure 8A). The Val32 side chain does not extend as far into the FMN pocket as Leu and thereby provides more conformational freedom for Cys55. In general, the Leu32Val substitution appears to destabilize the protein structure surrounding the active site Cys: the loop regions have opened, they are more mobile, and the Cys is less conformationally constrained. These factors all likely contribute to the increased reversion rates.

Structure and Solution Behavior of the A138Y RsLOV Variant. We also produced a variant RsLOV designed to alter the dimer interface in the dark state by mutating one of the Ala repeat residues at the center of the Jα helix interface to Tyr. The structure of the A138Y RsLOV variant was determined

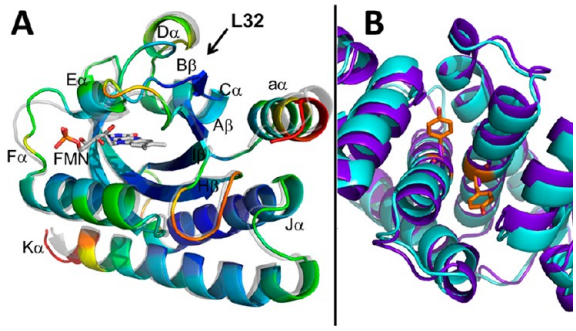

Figure 8. Structures of L32V and A138Y RsLOV. (A) Structure of the L32V RsLOV variant in the dark state colored by *B* factor (ROYGBIV spectrum coloring in which red is the maximum and violet is the minimum) overlaid on the $P6_5$ dark-state RLOV structure (gray, transparent). (B) Structure of the A138Y RsLOV variant in the dark state (aqua) overlaid on the $P6_5$ dark-state RsLOV structure (violet). The dimer interface is unperturbed by change of Ala138 (violet sticks) to Tyr (orange sticks).

from a single crystal that formed under the same crystallization conditions that were used for the WT. Despite the same conditions, the hexagonal crystal was distinctly conical in shape in contrast to the long rods that formed from the WT. However, the crystallographic data scaled to the $P6_5$ space group, with unit cell dimensions (a = 105.9 Å, b = 105.9 Å, c = 84.1 Å, α = 90°, β = 90°, and γ = 120°) similar to those of the WT. The structure is the same crystallographic dimer as that of the WT, with the Tyr side chains forced alongside the Jα helical interface (Figure 8B). Despite the introduction of the bulky Tyr residues at the dimer interface, the A138Y structure produces a subunit association nearly identical to that of the WT RsLOV structure. There are no significant deviations of the path or direction of the Jα or Kα helices at the interface, and no conformational changes that propagate from the single-residue change. Thus, crystallization strongly favors the dark-state dimer, and the crystal packing forces are able to overcome a substantial perturbation to the interface. The curve generated via SEC of A138Y is included in Figure S3 of the Supporting Information and indicates that this substitution, designed to disrupt the dimer interface, in fact, predisposes the variant to form a dimer in solution. Tyrosine is well suited for mediating molecular recognition at protein−protein interfaces,[80] because tyrosine uses interactions of both the side chain hydroxyl and the aromatic ring to make specific contacts with a wide variety of residues on a protein surface. Thus, despite the large increase in side chain volume at the interface, for these other reasons, Tyr138 facilitates RsLOV dimerization. Moreover, there is no significant change to the A138Y variant in solution upon its exposure to light, indicating that this variant interferes with the propagation of the signal from the PAS core to the flanking helices.

DISCUSSION

RsLOV is a LOV domain protein that has a moderate lifetime (2374 s) for the cysteinyl−flavin adduct state. The striking aspects of the RsLOV structure are its short N-terminal helical extension and its long C-terminal HTH dimerization motif. In the crystal structure, two RsLOV subunits pack together through the C-terminal HTH motifs to form a closely associated four-helix bundle, flanked by the N-terminal helices. A preponderance of Gly and Ala residues in the interface generates a tight knitting of the Jα helices. Evidence from

dx.doi.org/10.1021/bi3015373 | *Biochemistry* 2013, 52, 378−391

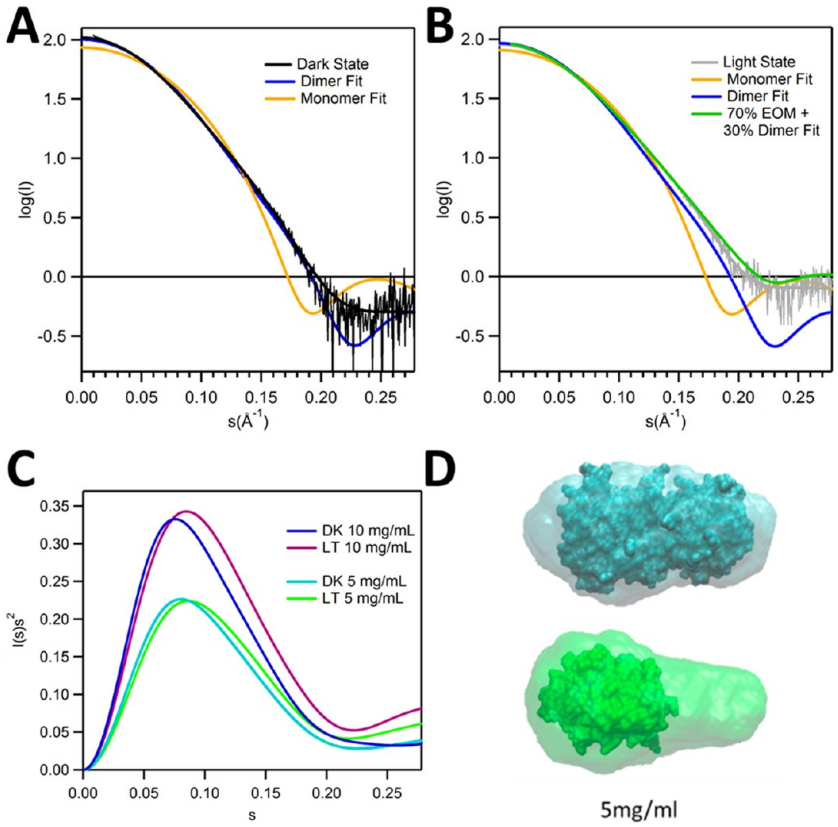

Figure 9. SAXS of RsLOV in dark and light states. (A) Fits of scaled theoretical monomer (orange) and dimer (blue) scattering curves generated with CRYSOL for the dark-state (black) and (B) light-state (gray) RsLOV (5 mg/mL data). EOM fits generated with RANCH13/GAJOE13 of the monomer were generated from the truncated PDB file of the dimer with only the A subunit. Light-state fit composed of 70% EOM monomer model and 30% dimer (lime). (C) Kratky plot of dark- and light-state RsLOV data of 10 and 5 mg/mL samples. (D) Scattering envelope models based on the 5 mg/mL SAXS data of dark-state RsLOV (top, cyan) and light-state RsLOV (bottom, green), superimposed with the crystal structure surface of RsLOV, as a complete dimer or truncated to a monomer.

chromatographic, light scattering, and chemical cross-linking indicates that light causes the RsLOV dimer to dissociate. This behavior is in marked contrast to that of VVD, where light causes dimerization. The structural changes determined from the light-state X-ray crystal structure suggest that despite its unusual oligomerization, RsLOV behaves like other well-characterized LOV domain proteins, such as AsLOV2 (LOV2 domain protein of oat), with which it shares a long flanking Jα helix. Although irradiation of the dark-state crystals produces few large-scale structural perturbations, difference Fourier analysis indicates that conformational changes propagate from the flavin N5 position, through the conserved Gln amide, across Iβ to the Ncap and Jα, which lie against the PAS β-sheet. These structural changes must ultimately disrupt contacts in the helical dimer interface and lead to subunit dissociation.

The study of several RsLOV variants revealed that minor perturbations in side chain size or polarity have minor effects on adduct stability. Mutations localized to the FMN binding pocket destabilized the Cys−FMN adduct and increased the rate of thermal reversion. The most impactful mutation was the L32V mutation, which increased the recovery rate 14-fold. The crystallographic structure of L32V RsLOV showed that a conservative point mutation in a small, compact domain can induce extensive structural changes. The substitution of Leu32 located in the Bβ strand altered the positioning of helices Dα and Eα and the flexible connecting loops on the *si* face of the FMN. These changes likely cause increased domain dynamics that result in destabilization of the adduct bond and greater solvent accessibility of flavin N5 to aid in the deprotonation.

Blue-Light-Induced Structural Changes. The changes exhibited in the light-state RsLOV crystal structure, obtained from irradiation of dark-state RsLOV crystals, capture the initial structural perturbations induced by adduct formation, which was visualized in one of the two independent subunits. The majority of residues impacted by the light in the crystal structure are within the first sphere of residues of the FMN binding pocket. These residues, highlighted by the changes in the $F_o - F_c$ omit maps between the light and dark states, include Cys55 and Gln118, which have been shown in other LOV domains to be critical for altering hydrogen bonding in the flavin binding pocket and thereby causing the predicted large conformational changes. Second-sphere residues in the solvent-exposed regions also highlighted by the difference Fourier analysis include Ala133 in the Jα helix, Arg10 and F13 in the aα helix, and Gly48 and Leu51 in the Dα helix. Differences in the density surrounding the Jα helix of AsLOV2 indicate that movement of the Jα helix is an initial response in RsLOV, as it is in other LOV domains.[72,81] Indeed, the integrity of the tightly packed helical interface of RsLOV may be especially sensitive to small changes in the position of Jα. The subunit contact relies on having virtually no side chain contribution at the center of the interface, and such an association would be incompatible with a slight shift or rotation of helix Jα.

dx.doi.org/10.1021/bi3015373 | *Biochemistry* 2013, 52, 378−391

Blue-Light Signal Propagation in *R. sphaeroides*. Although large structural rearrangements in the RsLOV light state will be prevented by crystal packing constraints and the short-lived adduct state precludes a long-lived, crystallizable intermediate, the differences observed between the light- and dark-state RsLOV structures in illuminated crystals reveal structural perturbations that suggest a larger rearrangement involving the N- and C-terminal flanking regions. It is interesting that the SAXS scattering profiles of the light-excited samples are not particularly well modeled from linear combinations of the monomer and dimer scattering profiles, as calculated from the crystal structure, and are better modeled by designating regions of disorder. One explanation for this is that the dissociated RsLOV monomer changes conformation considerably from how it appears in the dimer crystal structure.

In a recent SAXS study of light-induced movement of the LOV2 domain in *Arabidopsis* phot2, the linker region that is responsible for executing the light-induced conformational changes between the LOV2 and kinase domains is Jα helix-like.[82] The SAXS profiles suggest photoreversible movement of the LOV domain with a Jα linker relative to the effector domain, which produces a more extended structure in the light state.[82] Molecular dynamics studies of AsLOV2 revealed a partial unfolding of the Jα helix, which precedes its detachment from the LOV2 domain interface, a rearrangement originally proposed from the initial structural characterization of AsLOV2.[71,72,81] The RsLOV residues attributed to the partial unfolding of the Jα helix (Ile533−Ile539, centrally located residues adjacent to Gln513 of the Iβ strand) are similarly affected in the observed structural changes from the dark to light state in RsLOV crystals (Ala133 adjacent to Gln118). Thus, a large conformational change is also possible in the RsLOV protein that would extend the Jα and Kα helices away from the LOV domain. The SAXS data suggest that this may indeed be the case (Figure 9C).

RsLOV Flanking Regions. The N- and C-terminal extensions of RsLOV flank the LOV domain core where they are held in place by hydrophobic interactions and side chain-mediated hydrogen bonds. The long C-terminal extension of RsLOV is a unique HTH motif (Jα and Kα) that has not been observed previously in LOV domain proteins and forms an unusual dimerization domain. A Dali search[83] of the dimerization domain finds only weak structural homology to other coiled coils. The topology and juxtaposition of helices Jα and Kα are most similar to those of the membrane helices found in mechanosensitive channels, membrane transporters, and the transducer of sensory rhodopsin, but the relationships are only approximate (Figure 10). To the best of our knowledge, the tight interaction between Jα helices and helical crossing angles at the interface has not been previously observed. The overall domain architecture of RsLOV is perhaps similar to that of EL222, which has a DNA-binding HTH effector domain coordinated to the LOV domain via a Jα helix, but the HTH motif of EL222 consists of shorter helices that are arranged differently, do not flank the LOV core, and do not dimerize.[47] However, the EL222 HTH motif does respond to light, which alters the ability of the protein to bind DNA.

Perhaps the most relevant analogues of RsLOV are the bacterial sensory rhodopsin (sR) light sensors, which are membrane proteins that convert light signals to conformational changes in a helical transducer protein. The coupling module of the transducer is a membrane-embedded four-helix bundle, composed of two antiparallel helices from each subunit.[84,85] On the periphery of each helical hairpin are two transmembrane sR proteins. Isomerization of the retinal cofactor in sR is thought to perturb the orientation of the transducer helices, thereby sending conformational signals through their cytoplasmic HAMP domains.[86] The sR units are similar in size to that of the RsLOV PAS domains, and the transducer helices are oriented like helices Jα and Kα within each subunit. One of the key interface Gly residues and its flanking sequence of RsLOV are also found in the transducer. Thus, RsLOV may be seen as a soluble, functional analogue of bacterial sensory rhodopsin. The sR transducer remains a dimer throughout signal transduction, but the subunit association is stabilized by extensive interactions in the cytoplasmic regions. Without these additional regions, shifts in the RsLOV helices induced by the light-sensing PAS domains destabilize the dimeric interface enough to cause subunit dissociation.

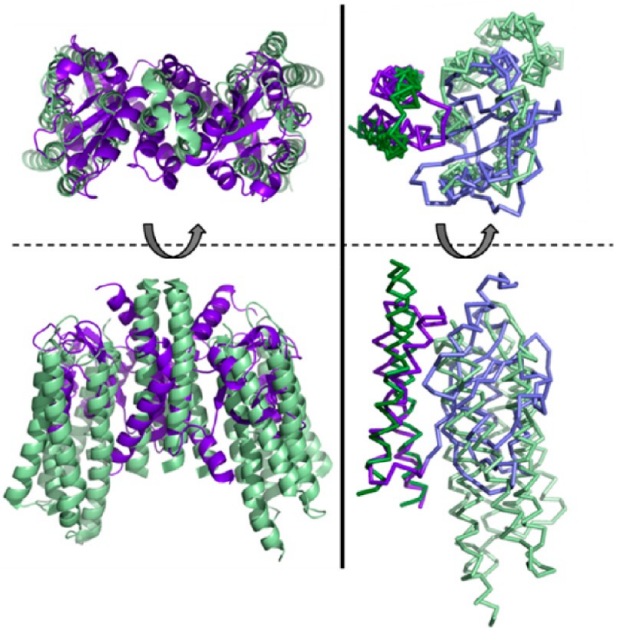

Figure 10. Analogy between RsLOV and sensory rhodopsin. The left panels show a structure of the RsLOV dimer (violet) overlaid on the dimer of sensory rhodopsin II in complex with the helical transducer (pale green, PDB entry 1H2S). The right panels show an overlay of the monomers of RsLOV and sensory rhodopsin II depicted as ribbons with the C-terminal helices aligned and colored darker than the PAS core and transducer helix bundle.

The RsLOV N-terminal extension may also play an important role in the light-induced subunit association and subsequent recognition of another protein, yet to be defined. The RsLOV N-terminal extension is a short aα helix that lacks the long flexible region that allows light-induced dimerization of VVD. The aα helix also flanks the LOV core and is held in place by hydrogen bonding with the Jα helix and hydrophobic interactions with the core β-strands. Arg10 and Phe13 of the N-terminal aα helix are perturbed when the adduct is formed in a manner similar to that of the second-sphere residue in the Jα helix. VVD undergoes a large structural rearrangement of the N-terminal extension upon conversion to the light state, but the RsLOV N-terminal extension lacks the flexible hinge regions preceding the LOV domain that transduce the conformational change in VVD. However, the role of the shorter aα helix in AsLOV2 has also recently been examined and was identified as a possible control element for use in optogenetic studies.[87] The

dx.doi.org/10.1021/bi3015373 | *Biochemistry* 2013, 52, 378−391

structural changes observed in the RsLOV aα helix may indicate that the helix is forced away from the LOV domain in a manner similar to that seen with the AsLOV2 Jα helix: first by distorting the helix at its center, which in turn disrupts the hydrophobic interactions that stabilize the aα helix against the surface of the PAS β-sheet. Were the Jα helix to unwind and release from the core like that of AsLOV2, the aα helix would likely follow, and its new conformation would act as a recognition site for a signaling partner.

Targets and interacting partners of RsLOV are currently unknown. The structural analogy between the RsLOV dimerization domain and the membrane helices of channels, photosensory transducers, and transporters raises the possibility that the target for these helices, once the RsLOV dimer is dissociated by light, is a similar set of helices, perhaps in or associated with the membrane. Previous studies of RsLOV from *R. sphaeroides* 2.4.1 detected the protein in both the cytoplasm and the membrane fractions,[39] making a signal to a transporter or a channel protein not unreasonable. RsLOV has been linked to a regulatory role in photosynthetic gene expression, carbohydrate metabolism, chemotaxis, and the response to photooxidative stress.[51] RsLOV also impacts blue-light-dependent gene expression and redox-dependent regulation.

LOV domain proteins are rapidly being designed and applied as tools in the emerging field of optogenetics.[29,88−90] RsLOV offers new utility as a photoswitch with a unique combination of features for controlling cellular processes. These properties include the ability to switch from dimer to monomer upon exposure to light, as well as both N- and C-terminal helical extensions whose conformations change on release and may thereby serve as sites for new protein interactions. Moreover, the change in the oligomeric state of RsLOV can be manipulated by mutation. Applications could include oligomers of designed RsLOV domains that cage or localize interactions to be released by photoactivation and controlled conformational switching of attached segments with either N- or C-terminal coupling.

■ ASSOCIATED CONTENT

Ⓢ Supporting Information

Structural and refinement statistics for crystallographic data, data obtained by SEC−MALS and analytical SEC, SAXS data and shape reconstruction statistics, and data from cross-linking experiments. This material is available free of charge via the Internet at http://pubs.acs.org.

■ AUTHOR INFORMATION

Corresponding Author

*Baker Laboratory, Ithaca, NY 14853-1301. Phone: (607) 255-8634. Fax: (607) 255-1248. E-mail: bc69@cornell.edu.

Author Contributions

The manuscript was written through contributions of all authors. All authors have given approval to the final version of the manuscript.

Funding

This work was supported by National Institutes of Health (NIH) Grant GM079679 to B.R.C. and NIH Grant FGM099391A to K.S.C.

Notes

The authors declare no competing financial interest.

■ ACKNOWLEDGMENTS

We thank the Cornell High Energy Synchrotron Source (CHESS) for access to data collection facilities. We also thank J. Widom for help with mutagenesis and protein expression and L. J. Byrnes for assistance with MALS.

■ ABBREVIATIONS

LOV, light−oxygen−voltage; PAS, Per-ARNT-Sim; FMN, flavin mononucleotide; FAD, flavin adenine dinucleotide; SAXS, small-angle X-ray scattering; phot, phototropin; EL, *Er. litoralis*; As, *A. sativa*; Pp, *P. putida*; VVD, VIVID; HTH, helix−turn−helix; sR, sensory rhodopsin; EOM, ensemble optimization method; MW, molecular weight.

■ REFERENCES

(1) Taylor, B., and Zhulin, I. (1999) PAS domains: Internal sensors of oxygen, redox potential, and light. *Microbiol. Mol. Biol. Rev. 63*, 479.

(2) Ayers, R., and Moffat, K. (2008) Changes in Quaternary Structure in the Signaling Mechanisms of PAS Domains. *Biochemistry 47*, 12078−12086.

(3) Möglich, A., Ayers, R. A., and Moffat, K. (2009) Structure and Signaling Mechanism of Per-ARNT-Sim Domains. *Structure 17*, 1282−1294.

(4) Herrou, J., and Crosson, S. (2011) Function, structure and mechanism of bacterial photosensory LOV proteins. *Nat. Rev. Microbiol. 9*, 713−723.

(5) Christie, J. M., Salomon, M., Nozue, K., Wada, M., and Briggs, W. R. (1999) LOV (light, oxygen, or voltage) domains of the blue-light photoreceptor phototropin (nph1): Binding sites for the chromophore flavin mononucleotide. *Proc. Natl. Acad. Sci. U.S.A. 96*, 8779−8783.

(6) Salomon, M., Christie, J. M., Knieb, E., Lempert, U., and Briggs, W. R. (2000) Photochemical and mutational analysis of the FMN-binding domains of the plant blue light receptor, phototropin. *Biochemistry 39*, 9401−9410.

(7) Kottke, T., Dick, B., Fedorov, R., Schlichting, I., Deutzmann, R., and Hegemann, P. (2003) Irreversible photoreduction of flavin in a mutated Phot-LOV1 domain. *Biochemistry 42*, 9854−9862.

(8) Kottke, T., Heberle, J., Hehn, D., Dick, B., and Hegemann, P. (2003) Phot-LOV1: Photocycle of a Blue-Light Receptor Domain from the Green Alga *Chlamydomonas reinhardtii*. *Biophys. J. 84*, 1192−1201.

(9) Kasahara, M., Swartz, T. E., Olney, M. A., Onodera, A., Mochizuki, N., Fukuzawa, H., Asamizu, E., Tabata, S., Kanegae, H., Takano, M., Christie, J. M., Nagatani, A., and Briggs, W. R. (2002) Photochemical properties of the flavin mononucleotide-binding domains of the phototropins from *Arabidopsis*, rice, and *Chlamydomonas reinhardtii*. *Plant Physiol. 129*, 762−773.

(10) Briggs, W. R., and Huala, E. (1999) Blue-light photoreceptors in higher plants. *Annu. Rev. Cell Dev. Biol. 15*, 33−62.

(11) Jain, M., Sharma, P., Tyagi, S. B., Tyagi, A. K., and Khurana, J. P. (2007) Light regulation and differential tissue-specific expression of phototropin homologues from rice (*Oryza sativa* ssp indica). *Plant Sci. 172*, 164−171.

(12) Purcell, E. B., Siegal-Gaskins, D., Rawling, D. C., Fiebig, A., and Crosson, S. (2007) A photosensory two-component system regulates bacterial cell attachment. *Proc. Natl. Acad. Sci. U.S.A. 104*, 18241−18246.

(13) Purcell, E. B., McDonald, C. A., Palfey, B. A., and Crosson, S. (2010) An Analysis of the Solution Structure and Signaling Mechanism of LovK, a Sensor Histidine Kinase Integrating Light and Redox Signals. *Biochemistry 49*, 6761−6770.

(14) Aravind, L., and Koonin, E. V. (2000) The STAS domain: A link between anion transporters and anti-sigma-factor antagonists. *Curr. Biol. 10*, R53−R55.

(15) Buttani, V., Losi, A., Eggert, T., Krauss, U., Jaeger, K., Cao, Z., and Gärtner, W. (2007) Conformational analysis of the blue-light sensing protein YtvA reveals a competitive interface for LOV−LOV

dimerization and interdomain interactions. *Photochem. Photobiol. Sci. 6*, 41−49.
(16) Losi, A., Quest, B., and Gartner, W. (2003) Listening to the blue: The time-resolved thermodynamics of the bacterial blue-light receptor YtvA and its isolated LOV domain. *Photochem. Photobiol. Sci. 2*, 759−766.
(17) Möglich, A., and Moffat, K. (2007) Structural basis for light-dependent signaling in the dimeric LOV domain of the photosensor YtvA. *J. Mol. Biol. 373*, 112−126.
(18) Schwerdtfeger, C., and Linden, H. (2003) VIVID is a flavoprotein and serves as a fungal blue light photoreceptor for photoadaptation. *EMBO J. 22*, 4846−4855.
(19) Vaidya, A. T., Chen, C. H., Dunlap, J. C., Loros, J. J., and Crane, B. R. (2011) Structure of a Light-Activated LOV Protein Dimer That Regulates Transcription. *Sci. Signaling 4*, ra50.
(20) Zoltowski, B. D., and Crane, B. R. (2008) Light activation of the LOV protein Vivid generates a rapidly exchanging dimer. *Biochemistry 47*, 7012−7019.
(21) Zoltowski, B. D., Schwerdtfeger, C., Widom, J., Loros, J. J., Bilwes, A. M., Dunlap, J. C., and Crane, B. R. (2007) Conformational switching in the fungal light sensor vivid. *Science 316*, 1054−1057.
(22) Zoltowski, B. D., Vaccaro, B., and Crane, B. R. (2009) Mechanism-based tuning of a LOV domain photoreceptor. *Nat. Chem. Biol. 5*, 827−834.
(23) Crosson, S., Rajagopal, S., and Moffat, K. (2003) The LOV domain family: Photoresponsive signaling modules coupled to diverse output domains. *Biochemistry 42*, 2−10.
(24) Losi, A. (2007) Flavin-based blue-light photosensors: A photobiophysics update. *Photochem. Photobiol. 83*, 1283−1300.
(25) Circolone, F., Granzin, J., Jentzsch, K., Drepper, T., Jaeger, K. E., Willbold, D., Krauss, U., and Batra-Safferling, R. (2012) Structural Basis for the Slow Dark Recovery of a Full-Length LOV Protein from *Pseudomonas putida*. *J. Mol. Biol. 417*, 362−374.
(26) Chen, C. H., DeMay, B. S., Gladfelter, A. S., Dunlap, J. C., and Loros, J. J. (2010) Physical interaction between VIVID and white collar complex regulates photoadaptation in *Neurospora*. *Proc. Natl. Acad. Sci. U.S.A. 107*, 16715−16720.
(27) Hunt, S. M., Thompson, S., Elvin, M., and Heintzen, C. (2010) VIVID interacts with the WHITE COLLAR complex and FREQUENCY-interacting RNA helicase to alter light and clock responses in Neurospora. *Proc. Natl. Acad. Sci. U.S.A. 107*, 16709−16714.
(28) Malzahn, E., Ciprianidis, S., Káldi, K., Schafmeier, T., and Brunner, M. (2010) Photoadaptation in *Neurospora* by Competitive Interaction of Activating and Inhibitory LOV Domains. *Cell 142*, 762−772.
(29) Strickland, D., Yao, X. L., Gawlak, G., Rosen, M. K., Gardner, K. H., and Sosnick, T. R. (2010) Rationally improving LOV domain-based photoswitches. *Nat. Methods 7*, 623−626.
(30) Erbel, P. J. A., Card, P. B., Karakuzu, O., Bruick, R. K., and Gardner, K. H. (2003) Structural basis for PAS domain heterodimerization in the basic helix-loop-helix-PAS transcription factor hypoxia-inducible factor. *Proc. Natl. Acad. Sci. U.S.A. 100*, 15504−15509.
(31) Lee, J., Tomchick, D. R., Brautigam, C. A., Machius, M., Kort, R., Hellingwerf, K. J., and Gardner, K. H. (2008) Changes at the KinA PAS-A dimerization interface influence histidine kinase function. *Biochemistry 47*, 4051−4064.
(32) Salomon, M., Lempert, U., and Rudiger, W. (2004) Dimerization of the plant photoreceptor phototropin is probably mediated by the LOV1 domain. *FEBS Lett. 572*, 8−10.
(33) Miyatake, H., Mukai, M., Park, S. Y., Adachi, S., Tamura, K., Nakamura, H., Nakamura, K., Tsuchiya, T., Iizuka, T., and Shiro, Y. (2000) Sensory mechanism of oxygen sensor FixL from *Rhizobium meliloti*: Crystallographic, mutagenesis and resonance Raman spectroscopic studies. *J. Mol. Biol. 301*, 415−431.
(34) Key, J., Hefti, M., Purcell, E. B., and Moffat, K. (2007) Structure of the redox sensor domain of *Azotobacter vinelandii* NifL at atomic resolution: Signaling, dimerization, and mechanism. *Biochemistry 46*, 3614−3623.
(35) Kurokawa, H., Lee, D. S., Watanabe, M., Sagami, I., Mikami, B., Raman, C. S., and Shimizu, T. (2004) A redox-controlled molecular switch revealed by the crystal structure of a bacterial heme PAS sensor. *J. Biol. Chem. 279*, 20186−20193.
(36) Jurk, M., Dorn, M., and Schmieder, P. (2011) Blue Flickers of Hope: Secondary Structure, Dynamics, and Putative Dimerization Interface of the Blue-Light Receptor YtvA from *Bacillus subtilis*. *Biochemistry 50*, 8163−8171.
(37) Möglich, A., Ayers, R. A., and Moffat, K. (2010) Addition at the Molecular Level: Signal Integration in Designed Per-ARNT-Sim Receptor Proteins. *J. Mol. Biol. 400*, 477−486.
(38) King, H. A., Hoelz, A., Crane, B. R., and Young, M. W. (2011) Structure of an Enclosed Dimer Formed by the *Drosophila* Period Protein. *J. Mol. Biol. 413*, 561−572.
(39) Hendrischk, A. K., Moldt, J., Fruhwirth, S. W., and Klug, G. (2009) Characterization of an Unusual LOV Domain Protein in the α-Proteobacterium *Rhodobacter sphaeroides*. *Photochem. Photobiol. 85*, 1254−1259.
(40) Hendrischk, A. K., Fruhwirth, S. W., Moldt, J., Pokorny, R., Metz, S., Kaiser, G., Jager, A., Batschauer, A., and Klug, G. (2009) A cryptochrome-like protein is involved in the regulation of photosynthesis genes in *Rhodobacter sphaeroides*. *Mol. Microbiol. 74*, 990−1003.
(41) Pairwise scores are percentages that represent the number of identities between the two sequences divided by the length of the alignment.
(42) Alexandre, M. T., Arents, J. C., van Grondelle, R., Hellingwerf, K. J., and Kennis, J. T. (2007) A base-catalyzed mechanism for dark state recovery in the *Avena sativa* phototropin-1 LOV2 domain. *Biochemistry 46*, 3129−3137.
(43) Larkin, M. A., Blackshields, G., Brown, N. P., Chenna, R., McGettigan, P. A., McWilliam, H., Valentin, F., Wallace, I. M., Wilm, A., Lopez, R., Thompson, J. D., Gibson, T. J., and Higgins, D. G. (2007) ClustalW and ClustalX version 2.0. *Bioinformatics 23*, 2947−2948.
(44) Goujon, M., McWilliam, H., Li, W., Valentin, F., Squizzato, S., Paern, J., and Lopez, R. (2010) A new bioinformatics analysis tools framework at EMBL−EBI. *Nucleic Acids Res. 38* (Suppl.), W695−W699.
(45) Jentzsch, K., Wirtz, A., Circolone, F., Drepper, T., Losi, A., Gärtner, W., Jaeger, K.-E., and Krauss, U. (2009) Mutual Exchange of Kinetic Properties by Extended Mutagenesis in Two Short LOV Domain Proteins from *Pseudomonas putida*. *Biochemistry 48*, 10321−10333.
(46) Krauss, U., Losi, A., Gartner, W., Jaeger, K. E., and Eggert, T. (2005) Initial characterization of a blue-light sensing, phototropin-related protein from *Pseudomonas putida*: A paradigm for an extended LOV construct. *Phys. Chem. Chem. Phys. 7*, 2804−2811.
(47) Nash, A. I., McNulty, R., Shillito, M. E., Swartz, T. E., Bogomolni, R. A., Luecke, H., and Gardner, K. H. (2011) Structural basis of photosensitivity in a bacterial light-oxygen-voltage/helix-turn-helix (LOV-HTH) DNA-binding protein. *Proc. Natl. Acad. Sci. U.S.A. 108*, 9449−9454.
(48) Avila-Perez, M., Vreede, J., Tang, Y. F., Bende, O., Losi, A., Gartner, W., and Hellingwerf, K. (2009) In Vivo Mutational Analysis of YtvA from *Bacillus subtilis* Mechanism of Light Activation of the General Stress Rresponse. *J. Biol. Chem. 284*, 24958−24964.
(49) Möglich, A., Ayers, R. A., and Moffat, K. (2009) Design and Signaling Mechanism of Light-Regulated Histidine Kinases. *J. Mol. Biol. 385*, 1433−1444.
(50) Brunger, A. T., Adams, P. D., Clore, G. M., DeLano, W. L., Gros, P., Grosse-Kunstleve, R. W., Jiang, J. S., Kuszewski, J., Nilges, M., Pannu, N. S., Read, R. J., Rice, L. M., Simonson, T., and Warren, G. L. (1998) Crystallography & NMR system: A new software suite for macromolecular structure determination. *Acta Crystallogr. 54*, 905−921.
(51) Metz, S., Jager, A., and Klug, G. (2012) Role of a short light, oxygen, voltage (LOV) domain protein in blue light- and singlet

oxygen-dependent gene regulation in *Rhodobacter sphaeroides*. *Microbiology (Reading, U.K.) 158*, 368−379.
(52) Otwinowski, Z., and Minor, W. (1997) Processing of X-ray diffraction data collected in oscillation mode. In *Methods in Enzymology* (Carter, C. W., Jr., Ed.) pp 307−326, Academic Press, San Diego.
(53) Adams, P. D., Afonine, P. V., Bunkoczi, G., Chen, V. B., Davis, I. W., Echols, N., Headd, J. J., Hung, L.-W., Kapral, G. J., Grosse-Kunstleve, R. W., McCoy, A. J., Moriarty, N. W., Oeffner, R., Read, R. J., Richardson, D. C., Richardson, J. S., Terwilliger, T. C., and Zwart, P. H. (2010) PHENIX: A comprehensive Python-based system for macromolecular structure solution. *Acta Crystallogr. D66*, 213−221.
(54) McRee, D. E. (1992) XtalView: A visual protein crystallographic software system for X11/Xview. *J. Mol. Graphics 10*, 44−47.
(55) Afonine, P. V., Grosse-Kunstleve, R. W., Echols, N., Headd, J. J., Moriarty, N. W., Mustyakimov, M., Terwilliger, T. C., Urzhumtsev, A., Zwart, P. H., and Adams, P. D. (2012) Towards automated crystallographic structure refinement with phenix.refine. *Acta Crystallogr. 68*, 352−367.
(56) Ando, N., Chenevier, P., Novak, M., Tate, M. W., and Gruner, S. M. (2008) High hydrostatic pressure small-angle X-ray scattering cell for protein solution studies featuring diamond windows and disposable sample cells. *J. Appl. Crystallogr. 41*, 167−175.
(57) Nielsen, S. S., Toft, K. N., Snakenborg, D., Jeppesen, M. G., Jacobsen, J. K., Vestergaard, B., Kutter, J. P., and Arleth, L. (2009) BioXTAS RAW, a software program for high-throughput automated small-angle X-ray scattering data reduction and preliminary analysis. *J. Appl. Crystallogr. 42*, 959−964.
(58) Petoukhov, M. V., Konarev, P. V., Kikhney, A. G., and Svergun, D. I. (2007) ATSAS 2.1: Towards automated and web-supported small-angle scattering data analysis. *J. Appl. Crystallogr. 40*, S223−S228.
(59) Petoukhov, M. V., Franke, D., Shkumatov, A. V., Tria, G., Kikhney, A. G., Gajda, M., Gorba, C., Mertens, H. D. T., Konarev, P. V., and Svergun, D. I. (2012) New developments in the ATSAS program package for small-angle scattering data analysis. *J. Appl. Crystallogr. 45*, 342−350.
(60) Konarev, P. V., Volkov, V. V., Sokolova, A. V., Koch, M. H. J., and Svergun, D. I. (2003) PRIMUS: A Windows PC-based system for small-angle scattering data analysis. *J. Appl. Crystallogr. 36*, 1277−1282.
(61) Wriggers, W., and Chacon, P. (2001) Using Situs for the registration of protein structures with low-resolution bead models from X-ray solution scattering. *J. Appl. Crystallogr. 34*, 773−776.
(62) Fischer, H., Neto, M. D., Napolitano, H. B., Polikarpov, I., and Craievich, A. F. (2010) Determination of the molecular weight of proteins in solution from a single small-angle X-ray scattering measurement on a relative scale. *J. Appl. Crystallogr. 43*, 101−109.
(63) Svergun, D., Barberato, C., and Koch, M. H. J. (1995) CRYSOL: A program to evaluate X-ray solution scattering of biological macromolecules from atomic coordinates. *J. Appl. Crystallogr. 28*, 768−773.
(64) Bernadó, P., Mylonas, E., Petoukhov, M. V., Blackledge, M., and Svergun, D. I. (2007) Structural Characterization of Flexible Proteins Using Small-Angle X-ray Scattering. *J. Am. Chem. Soc. 129*, 5656−5664.
(65) Volkov, V. V., and Svergun, D. I. (2003) Uniqueness of ab initio shape determination in small-angle scattering. *J. Appl. Crystallogr. 36*, 860−864.
(66) Franke, D., and Svergun, D. I. (2009) DAMMIF, a program for rapid ab-initio shape determination in small-angle scattering. *J. Appl. Crystallogr. 42*, 342−346.
(67) Krissinel, E. (2009) Crystal contacts as nature's docking solution. *J. Comput. Chem. 31*, 133−143.
(68) Krissinel, E., and Henrick, K. (2007) Inference of Macromolecular Assemblies from Crystalline State. *J. Mol. Biol. 372*, 774−797.
(69) Fedorov, R., Schlichting, I., Hartmann, E., Domratcheva, T., Fuhrmann, M., and Hegemann, P. (2003) Crystal structures and molecular mechanism of a light-induced signaling switch: The Phot-LOV1 domain from *Chlamydomonas reinhardtii*. *Biophys. J. 84*, 2474−2482.
(70) Halavaty, A. S., and Moffat, K. (2007) N- and C-terminal flanking regions modulate light-induced signal transduction in the LOV2 domain of the blue light sensor phototropin 1 from *Avena sativa*. *Biochemistry 46*, 14001−14009.
(71) Peter, E., Dick, B., and Baeurle, S. A. (2010) Mechanism of signal transduction of the LOV2-J α photosensor from *Avena sativa*. *Nat. Commun. 1*, No. 122.
(72) Halavaty, A., and Moffat, K. (2007) N-and C-Terminal Flanking Regions Modulate Light-Induced Signal Transduction in the LOV2 Domain of the Blue Light Sensor Phototropin 1 from *Avena sativa*. *Biochemistry 46*, 14001−14009.
(73) Nash, A. I., Ko, W. H., Harper, S. M., and Gardner, K. H. (2008) A conserved glutamine plays a central role in LOV domain signal transmission and its duration. *Biochemistry 47*, 13842−13849.
(74) Jones, M. A., Feeney, K. A., Kelly, S. M., and Christie, J. M. (2007) Mutational analysis of phototropin 1 provides insights into the mechanism underlying LOV2 signal transmission. *J. Biol. Chem. 282*, 6405−6414.
(75) Freddolino, P. L., Dittrich, M., and Schulten, K. (2006) Dynamic switching mechanisms in LOV1 and LOV2 domains of plant phototropins. *Biophys. J. 91*, 3630−3639.
(76) Semenyuk, A. V., and Svergun, D. I. (1991) GNOM: A Program Package for Small-Angle Scattering Data-Processing. *J. Appl. Crystallogr. 24*, 537−540.
(77) Svergun, D. I. (1992) Determination of the Regularization Parameter In Indirect-Transform Methods Using Perceptual Criteria. *J. Appl. Crystallogr. 25*, 495−503.
(78) Philip, A. F., Kumauchi, M., and Hoff, W. D. (2010) Robustness and evolvability in the functional anatomy of a PER-ARNT-SIM (PAS) domain. *Proc. Natl. Acad. Sci. U.S.A. 107*, 17986−17991.
(79) Raffelberg, S., Mansurova, M., Gartner, W., and Losi, A. (2011) Modulation of the Photocycle of a LOV Domain Photoreceptor by the Hydrogen-Bonding Network. *J. Am. Chem. Soc. 133*, 5346−5356.
(80) Fellouse, F. A., Wiesmann, C., and Sidhu, S. S. (2004) Synthetic antibodies from a four-amino-acid code: A dominant role for tyrosine in antigen recognition. *Proc. Natl. Acad. Sci. U.S.A. 101*, 12467−12472.
(81) Harper, S. M., Neil, L. C., and Gardner, K. H. (2003) Structural basis of a phototropin light switch. *Science 301*, 1541−1544.
(82) Takayama, Y., Nakasako, M., Okajima, K., Iwata, A., Kashojiya, S., Matsui, Y., and Tokutomi, S. (2011) Light-Induced Movement of the LOV2 Domain in an Asp720Asn Mutant LOV2-Kinase Fragment of *Arabidopsis* Phototropin 2. *Biochemistry 50*, 1174−1183.
(83) Hasegawa, H., and Holm, L. (2009) Advances and pitfalls of protein structural alignment. *Curr. Opin. Struct. Biol. 19*, 341−348.
(84) Moukhametzianov, R., Klare, J. P., Efremov, R., Baeken, C., Goppner, A., Labahn, J., Engelhard, M., Buldt, G., and Gordeliy, V. I. (2006) Development of the signal in sensory rhodopsin and its transfer to the cognate transducer. *Nature 440*, 115−119.
(85) Gordeliy, V. I., Labahn, J., Moukhametzianov, R., Efremov, R., Granzin, J., Schlesinger, R., Buldt, G., Savopol, T., Scheidig, A. J., Klare, J. P., and Engelhard, M. (2002) Molecular basis of transmembrane signalling by sensory rhodopsin II-transducer complex. *Nature 419*, 484−487.
(86) Sasaki, J., Tsai, A.-I., and Spudich, J. L. (2011) Opposite Displacement of Helix F in Attractant and Repellent Signaling by Sensory Rhodopsin-Htr Complexes. *J. Biol. Chem. 286*, 18868−18877.
(87) Zayner, J. P., Antoniou, C., and Sosnick, T. R. (2012) The Amino-Terminal Helix Modulates Light-Activated Conformational Changes in AsLOV2. *J. Mol. Biol. 419*, 61−74.
(88) Lungu, O. I., Hallett, R. A., Choi, E. J., Aiken, M. J., Hahn, K. M., and Kuhlman, B. (2012) Designing Photoswitchable Peptides Using the AsLOV2 Domain. *Chem. Biol. 19*, 507−517.
(89) Hahn, K. M., and Kuhlman, B. (2010) Hold me tightly LOV. *Nat. Methods 7*, 595−597.
(90) Christie, J. M., Hitomi, K., Arvai, A. S., Hartfield, K. A., Mettlen, M., Pratt, A. J., Tainer, J. A., and Getzoff, E. D. (2012) Structural Tuning of the Fluorescent Protein iLOV for Improved Photostability. *J. Biol. Chem. 287*, 22295−22304.